Proceedings of the
International Conference on Mechanical Engineering and Renewable Energy 2017
(ICMERE2017) 18 – 20 December, 2017, Chittagong, Bangladesh

ICMERE2017-PI-000

ANALYSIS OF EFFECT OF ASPECT RATIO ON AIRFOIL PERFORMANCE

M. M. Hasan[1] and M. M. M. Talukder[2,*]

[1-2] Department of Mechanical Engineering, Chittagong University of Engineering & Technology, Chittagong-4349, Bangladesh.
mahmodh223@gmail.com[1], mehdi.cuet@gmail.com[2,*]

Abstract- *Aspect ratio of the airfoil is the ratio of wingspan to chord length. For an airfoil of having different aspect ratio will perform in a different way. The performance of an airfoil about axially asymmetric wings is a function of aspect ratio. The magnitudes of aerodynamic forces such as lift force and drag force will be changed due to a different angle of attack for individual aspect ratio. The shape of upper and lower curvatures from the mean cambered line is also being changed due to separate aspect ratio. As a result, the pressure force on the surfaces can change the field of the vortex generated around the flow separation region which may be another cause of the change of performance. Three samples of different aspect ratios such as AR=0.57, AR=0.62, and AR=0.67 of asymmetrical airfoils type NACA 2412 were tested both in numerically (CFD) and experimentally. Finally, the results show that the optimal performance was achieved at AR=0.57.*

Keywords: Lift force, Drag force, Aspect ratio, Computational fluid dynamics, *Airfoil*.

1. INTRODUCTION

With the advent of successful technology, the shape of the airfoil is being changed day by day to improve the performance of flight. In the period 1912–1918, the analysis of airplane wings took a giant step forward. Ludwig Prandtl and his colleagues showed that the aerodynamic consideration of wings could be split into two parts: (1) the study of the section of a wing—an airfoil—and (2) the modification of such airfoil properties to account for the complete, finite wing [1]. This approach is still used today; indeed, the theoretical calculation and experimental measurement of modern air-foil properties have been a significant part of the aeronautics research carried out by the National Aeronautics and Space Administration (NASA) in the 1970s and 1980s [1]. Chord length of an airfoil is the property of aspect ratio. The characteristics of aspect ratio can be changed by changing the chord length. On the other hand, the performance of airfoil is the function of aspect ratio. So, this analysis aims to find how the change of aspect ratio can be the subject of varying the efficient performance of airfoil.

2. THEORY

2.1 Lift Force

The lift force is the force generated perpendicular to the direction of travel for an object moving through a fluid (gas or liquid). The same effect occurs when a fluid moves over a stationary object, such as an airfoil in a wind tunnel. Airfoils are the most efficient shapes found so far that can generate lift while at the same time minimizing drag [3]. Lift force can be defined by Eq. (1),

$$F_L = C_L \, {}^1\!/_2 \, \rho V^2 A \qquad (1)$$

Where C_L is the lift coefficient, ρ is the density of air, V is the velocity, and A is the cross-sectional area.

2.2 Drag Force

The force a flowing fluid exerts on a body in the flow direction is called drag. The drag force is due to the combined effects of pressure and wall shear forces in the flow direction [2]. Drag force due to the combined effects of the wall shear stress and pressure forces is defined by Eq. (2)

$$F_D = C_D \, {}^1\!/_2 \, \rho V^2 A \qquad (2)$$

Where C_D is the drag coefficient, ρ is the density of air, V is the velocity, and A is the cross-sectional area.

2.3 Camber

Camber line of the airfoil is a property which defines upper and lower surfaces especially density of airfoil.

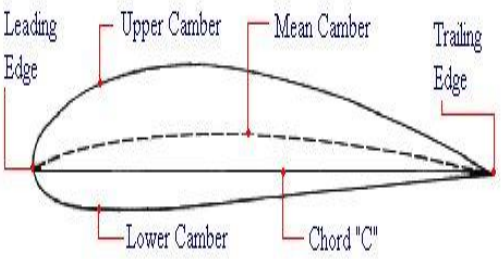

Fig.1: Cross-sectional view of an airfoil [4]

However, the most significant of it that camber line identifies the lift generated due to the flow of air around the floating body. For asymmetric airfoil, camber line depends on chord length which is the distance between the leading edge and the trailing edge shown in fig.1.

2.4 Computational Fluid Dynamics

Computational fluid dynamics (CFD) is a branch of fluid mechanics that uses numerical analysis and algorithms to solve and analyze problems that involve fluid flows. The most straightforward methods to understand are developed using numerical approximations to the derivative terms in the partial differential equation (PDE) form of the governing equations. Direct numerical solutions of the partial differential equations of fluid mechanics constitute the field of computational fluid dynamics (CFD) [5]. It allows the complex problems to solve for simulation.

2.5 Streamline

A streamline is an imaginary line drawn in a flow field such that a tangent drawn at any point on this line represents the direction of the velocity vector [2].

2.6 Vorticity

Vorticity is the measurement of rotation of a fluid particle. Specifically, vorticity is equal to twice the angular velocity of the fluid particle [6]. For airfoil and other high-speed vehicles, vorticity plays a vital role in varying the performance. This criterion is developed due to the irregular separation of flow from a higher pressure area to lower pressure area.

3. METHODOLOGY

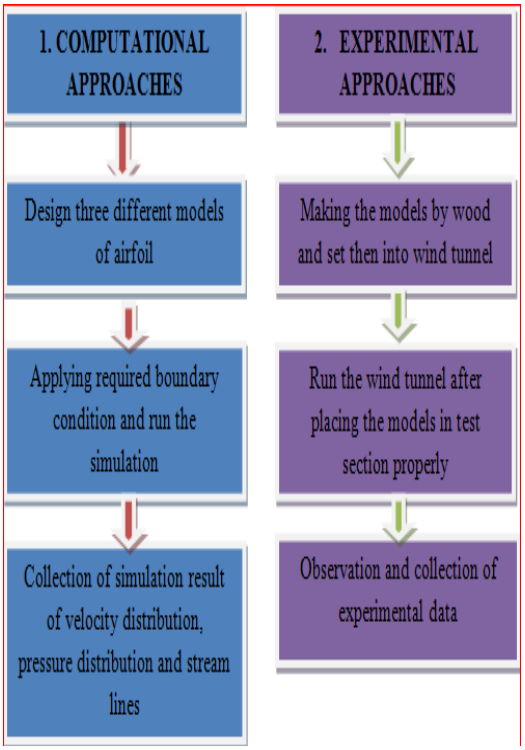

Fig.2: Flow chart of the methodology.

Both computational and experimental approaches are used to analyze the effect of aspect ratio on airfoil performance. The methodology of the analysis is shown above in a block diagram.

4. COMPUTATIONAL APPROACH

4.1 Design

In computational approach, the three models are designed using NACA2412 airfoil database in Solidworks 20114 (Student Version). These three models comprise constant wingspan (9.5cm) but different chord lengths such as 14.5cm, 15.5cm, and 16.5cm respectively. As a result, three different aspect ratio (AR=0.67, AR=0.61, and AR=0.57) are obtained. Then

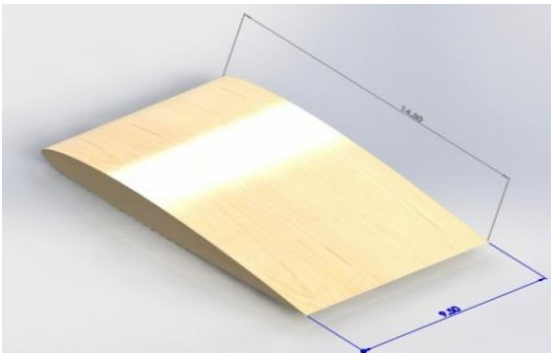

Fig. 3: Airfoil with 9.5cm wingspan and 14.5cm chord length (3D view).

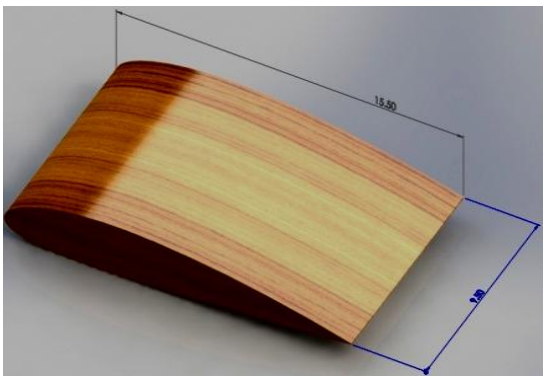

Fig.4: Airfoil with 9.5cm wingspan and 15.5cm chord length (3D view).

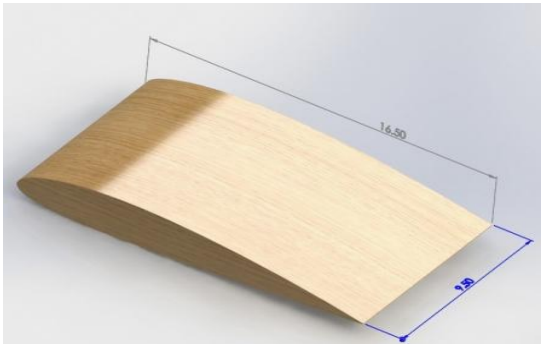

Fig. 5: Airfoil with 9.5cm wingspan and 16.5cm chord length (3D view).

creating geometry and meshing using the 2D cross-section of each model simulation are done. This provides the different options related to flow such as velocity distribution, pressure distribution, and streamlines profiles.

4.2 Geometry and Meshing

The numerical analysis of the models is accomplished using the ANSYS Fluent (Student Edition). Different planes were sketched for establishing the wall function by 3D physical designation. Three models comprise approximately similar structure shown in fig.5, but different in nodes and elements.

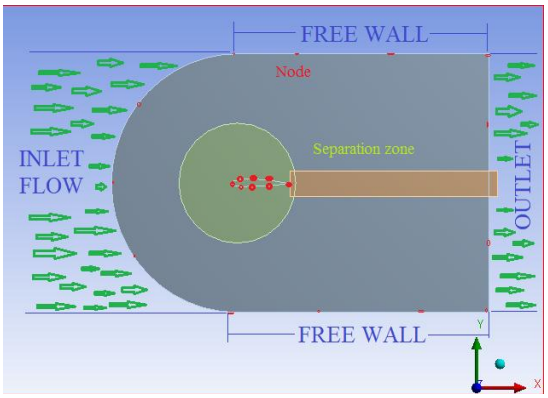

Fig.6: Geometry of the models.

Completing the geometry, the design module directly inputs for mesh .ANSYS automatic mesh generator chooses element sizes based on local curvature and edge length for all volumes.

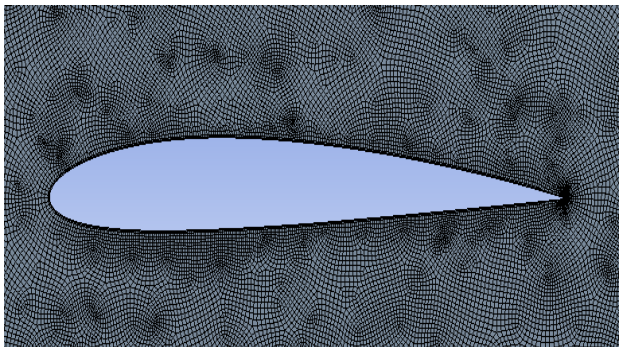

Fig.7: Mesh of AR=0.67

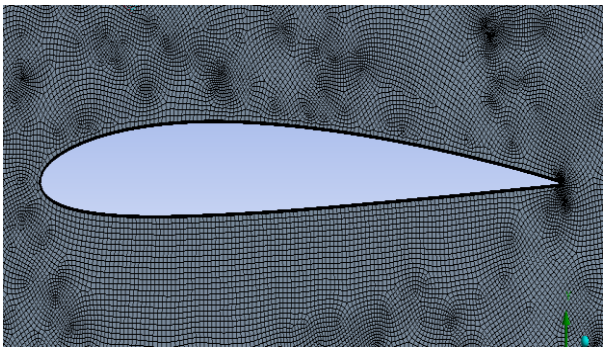

Fig.8: Mesh of AR=0.61

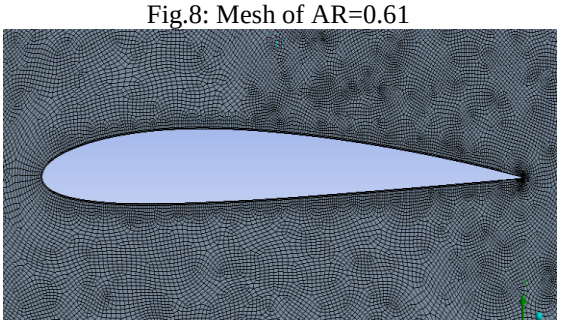

Fig. 9: Mesh of AR=0.57

Sizing is done through the programming controlled software. Maximum face size 0.10m, maximum size 0.10m and growth rate default (1.20). Inflation and disfeaturing are based on programming controlled. The geometry of the models is subdivided into different section such as inlet, outlet, and free wall. The mesh characteristics consist of 162224 nodes and 161696 elemental division of AR=0.67 whereas for AR=0.61, 176774 nodes, and 176366 elements and AR=0.57, consists of 112562 nodes and 112017 elements. The nodes and elemental divisions provide the guideline of visualization of the smoothness of transitional flow.

4.3 Fluent Visualization

The flow of particles around the body represents the pressure forces acting on the surfaces. For each model, the pressure differences between upper and lower surfaces generate the pressure drags and lift forces. Hence the performances can be observed individually.

From the fig.10, it is seen that the pressure on the upper surface is gradually increased due to the vorticity generation.

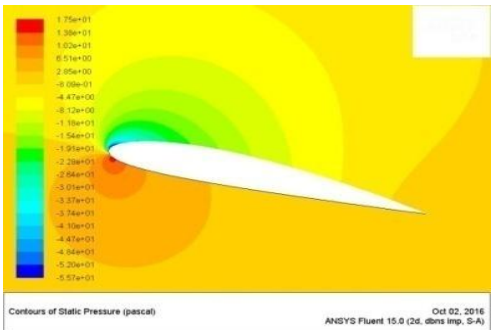

Fig.10: Pressure profile of AR=0.67 at the transition point.

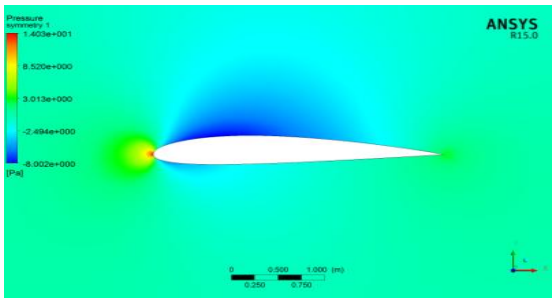

Fig.11: Pressure profile of AR=0.61 at transition point.

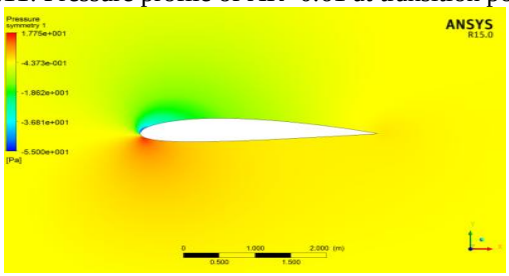

Fig.12: Pressure profile of AR=0.57 at the transition point.

As a result, the streamlines get obstacles to pass the body. Hence velocity and performance are not developed. However, in fig.10, it is clear that the pressure is reducing on the upper surface for lower aspect ratio. As a result, the drag force is reduced and lift being gradually increased.

On the other hand, the pressure on the upper surface gets very much reduced due to increasing the chord length, i.e., hence decreasing the aspect ratio in fig.11. In this point, the pressure forces acting on the lower surface increased dramatically causes a high lift generation. Flow particles get reduced obstacles. Thus the flow separation will be more smooth for model AR=0.57 compared to the AR=0.61 and AR=0.67. Hence the velocity and the performance will be increased. It refers to that the more pressure difference between the two surfaces for lower aspect ratio will make the airfoil more efficient.

5. EXPERIMENTAL APPROACH

In the experimental approach, first, three wooden models are prepared maintaining the dimensional constraints. Then holes are pierced in each wooden model to create pressure taps. Pressure data is collected by inserting plastic tubes in the holes and using multi-tube manometer. The experimental analysis was performed on an open type subsonic wind tunnel of a 0.355 m x 0.330 m x 0.380 m test section. The cross-sectional area of each models are 0.145m x 0.095= 0.0138m^2, 0.155m x 0.095m= 0.01473m^2 and 0.165m x 0.095=0.0157m^2. The three models were placed one after another inside the test section between the bell-mouthed contraction cone and the diffuser section. The loads were balanced for a different angle of attack according to the scale provided there.

Fig.13: Airfoil models with chord length 14.5cm.

Fig.14: Airfoil models with chord length 15.5cm.

Fig.15: Airfoil model with chord length 16.5cm.

Fig.16: Observation of manometric data during wind tunnel experiment.

Turning on the power switch, the speed of air flow through the inside section was controlled via speed regulator. In this type of wind tunnel, a multitube manometer was used for measuring the pressure difference through the variation of fluid (here kerosene oil) in the pressure tube.

5.1 Principle Equation

Specific gravity of air = 0.0013
Specific gravity of kerosene = 0.787
H_k=Pressure Head of Kerosene (m)
H_a= Pressure Head of Air (m)
Pressure head of Air,

$$Ha = (H_k \times (\frac{Sp.ofkerosene}{Sp.ofair} - 1))/ (1000 \times 1.5) \quad (m) \quad (3)$$

$$Pressure, P = H_a \times Density\ of\ Air \times g \quad (N/m^2) \quad (4)$$

$$Drag\ Force, F = P \times A \quad (N) \quad (5)$$

$$Coefficient\ of\ Drag, C_d = \frac{2 \times F}{Density \times Frontalarea \times velocity^2} \quad (6)$$

6. RESULTS AND DISCUSSION

6.1 Analysis of Computational Data

From the simulation, following criterions are found. The lift coefficient characteristics of the airfoil models under simulation are shown in Fig.17. The lift increases with increase in angle of attack to a maximum value and thereby decreases with further increase in angle of attack. For AR 0.57 the maximum value of the lift coefficient is 2.70, and this maximum values occur at an angle of attack of 16 degree. At the maximum angle of attack of 23 degree the lift coefficient is 2.49. The reason for a drop in lift coefficient beyond a particular angle of attack, e.g. 16 degree is due to the flow separation, which occurs over the wing surface instead of having a streamlined laminar flow there. This condition is called stalling condition, and the corresponding angle of attack is called stalling angle. The stalling angle happens to be approximately 16 degree. Other two curve for AR=0.61 and 0.67 are given in figure 16. Here from figure it is also seen that for AR=0.61 the maximum value of the lift coefficient is 2.4 at 18 degree AOA and for AR=0.67 the maximum value of the lift coefficient is 2.74 at 19 degree AOA. So from the figure, it is observed that for AR=0.57, the maximum value of lift coefficient is obtained at optimal AOA. The drag coefficient of the aircraft wing model under simulation is shown in Fig.18. The drag increases slowly with increase in angle of attack to a specific value and then it increases rapidly with further increase in angle of attack. The value of the drag coefficient at the transition point, i.e., at an angle of attack of 16 degree for AR=0.57 is 0.35, at 18° for AR=0.61 is 0.38 and at 19° for AR=0.67 is 0.47are respectively 0.35, 0.34 and 0.36. However, these values of 0.38 and 0.47 don't satisfy the lift coefficient at AOA 16 degree like AR=0.57. The simulations have been done up to 23-degree angle of attack. The rapid increase in drag coefficient, which occurs at higher values of angle of attack, is probably due to the increasing region of separated flow over the wing surface, which creates a substantial pressure drag. It is observed from the Fig.19, that the lift coefficient/drag coefficient ratio for all the configurations considered increases with an angle of attack to its maximum value, and thereby it decreases with further increase in angle of attack. In particular, it is observed that the maximum lift coefficient/drag coefficient ratio for all the configurations considered in the study falls in the range of 6 to 16 degrees of angle of attack. The airfoil model of AR 0.57 gives a measured lift coefficient/drag coefficient ratio of 17 whereas the respective values of the lift coefficient/drag coefficient ratio for the AR=0.61 and AR=0.67 are 14 and 13 respectively at an angle of attack of 6 degree. However, the lift coefficient/drag coefficient ratio values for the angle of attack of 16 degree are 7.3, 6.82 and 6.76 for airfoil model of AR 0.57, AR 0.61 and AR 0.67 respectively. From the above graphical representation, it is clear that the maximum lift force ($F_L=0.5\rho C_L V^2 A$) i.e.; maximum performance will be found through the model of AR=0.57 with an optimal AOA.

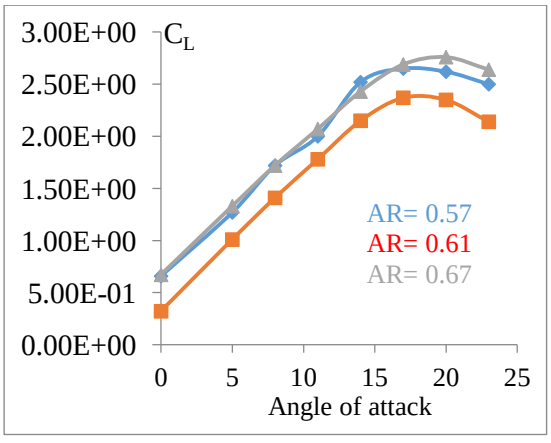

Fig.17: Lift Coefficient C_L vs. Angle of attack.

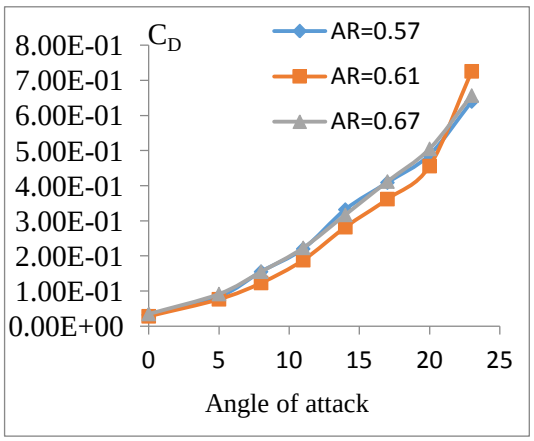

Fig. 18: Drag Coefficient C_D vs. angle of attack.

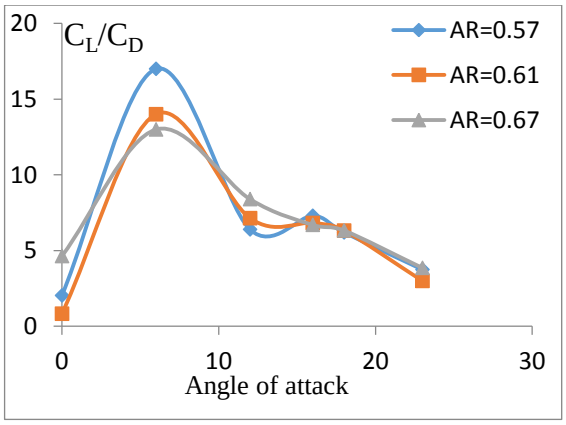

Fig.19: C_L/C_D vs. angle of attack.

6.2. Analysis of Experimental Data

From the experimental data, the curves for the lift coefficient vs. angle of attack and drag coefficient vs. angle of attack are as follows. From the fig.20, the highest lift coefficient of the airfoil of AR=0.57 is 0.62 at AOA of 12 degree. On the other hand, the maximum lift coefficient of AR=0.61 and AR=0.67 are 0.71 and 0.68 respectively at AOA of 18 degree. However, at the same time it can be noticed from fig.21, the drag coefficient of model AR=0.57 is 0.26 at 12 degree and for AR=0.61 and AR=0.67 the drag coefficients are 0.45 and 0.49 respectively at AOA of 18 degree. According to aerodynamic characteristics, the model which gives maximum lift force at an optimum angle of attack is more effective.

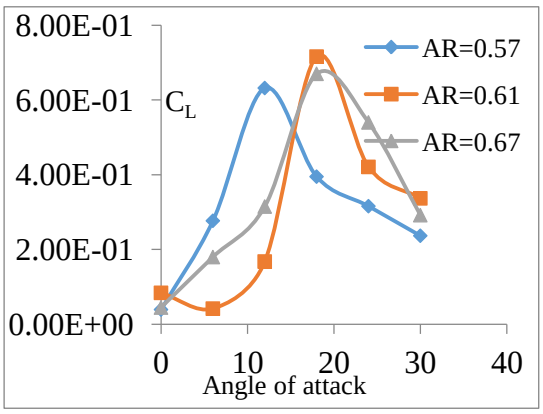

Fig.20: Lift coefficient vs. angle of attack.

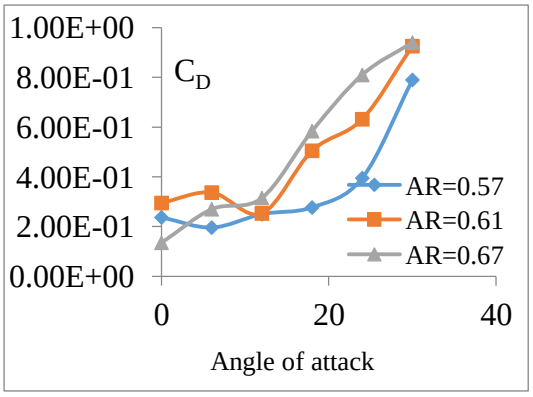

Fig. 21: Drag coefficient vs. angle of attack.

The maximum difference between lift coefficient and drag coefficient at highest lift angle of the three models [(0.62-0.26) =0.36 at 12° AOA of AR=0.57; (0.71-0.45) =0.26 at 18° AOA of AR=0.61; (0.67-0.49) =0.18 at 18° AOA of AR=0.67] will give maximum lift force to the respective model.

Again from fig.22, the maximum value of lift coefficient and drag coefficient ratio vs. angle of attack is 1.78 at 12° for the model AR=0.57. On the other hand, the similar values for models AR=0.61 and AR=0.67 are 1.40 and 1.18 respectively at 18° AOA. The maximum

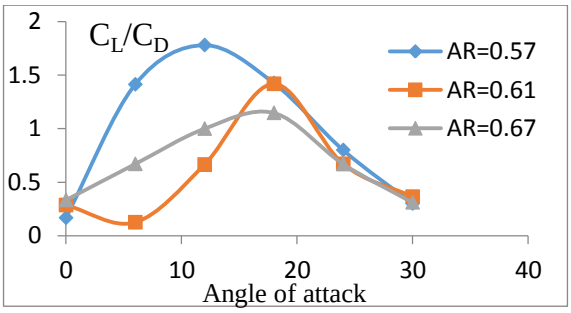

Fig.22: C_L/C_D vs. angle of attack.

value of CL/CD also indicates the high performance of airfoil. So, it can be concluded that, the model with aspect ratio 0.57 will give most efficient performance.

7. NUMERICAL AND EXPERIMENTAL RESULTS

After the analysis of graphical representation for both numerical and experimental data, the performance order can be shown as AR=0.57> AR=0.61> AR=0.67. However, there are some differences between numerical and experimental values. In case of simulation, there are some problems regarding the control of mesh shape, size, and overall mesh quality. As a result, there are some errors in the simulation results. On the other hand, the wind tunnel used for this experiment was the manual type which is not mechanically hundred percent accurate. During the experiment, the balancing of the airfoil in due position was a matter of fact because of lacking proper tightening screw. The models were not perfect as these are made from wood and machined by hand. So, there is some error in experimental values also. Although there are differences between the simulation and experimental data the trend of both these data's were quite similar and can assess the performance of airfoil precisely.

8. CONCLUSION

Two distinct approaches to investigate the effect of aspect ratio on airfoil performance were presented. The combination of wind tunnel experiments and CFD computation give a better understanding of the airfoil performance. From the CFD analysis, we found the required values of lift coefficient, drag coefficient, and pressure coefficient. After plotting graph with these values, we observed the maximum lift coefficient and minimum drag coefficient. Then experimental wind tunnel investigations were done to validate the computational results. The indication of lift and drag coefficient represented the performance of the airfoil with respect to different aspect ratio for different angle of attack. Analyzing the experimental and computational results, it has been possible to state an acceptable result to show the effect of aspect ratio on airfoil performance. The comparison shows that the computed drag forces and pressure distributions agree well with the experimental values over the entire range of air velocities. However, the agreement with the drag coefficient varies, which appears to suggest a higher degree of dependency on the details included in the geometric modeling, grid quality and elements selection. However, the critical value, in either case, is falling well within the permissible range, confirming acceptance and promising an efficient performance of the proposed profile.

9. ACKNOWLEDGEMENT

This work was partially supported by the Department of Mechanical Engineering, Chittagong University of Engineering & Technology (CUET) as an undergraduate project.

10. REFERENCES

[1] John D. Anderson Jr, Fundamentals of Aerodynamics, McGraw-Hill Education, 5th Edition, February-2010

[2] S. Pal, Dr.S.M.H. Kabir, M. M. M. Talukder, "Aerodynamic analysis of a concept car model", Proceedings of the International Conference on Mechanical Engineering and Renewable Energy 2015 (ICMERE2015), Chittagong, Bangladesh, 26 – 29 November - 2015.

[3] http://www.symscape.com/lift-force-and-drag-force (December 18, 2016)

[4] http://www.allstar.fiu.edu (September 24, 2016)

[5] Russell M. Cummings, Applied Computational Aerodynamics: A Modern Engineering Approach, Cambridge University Press; 1st Edition, April -2015.

[6] S. K. Som, G. Biswas, Introduction to Fluid Mechanics and Fluid Machines, McGraw-Hill India, 3rd Edition, 2011.

11. NOMENCLATURE

Symbol	Meaning	Unit
F_L	Lift force	N
F_D	Drag force	N
C_L	Coefficient of lift	Dimensionless
C_D	Coefficient of drag	Dimensionless
$V\infty$	Free stream velocity	m/s
∞	Free stream density	kg/m^3
$\mu\infty$	Free stream viscosity	m/s
α	Angle of attack (AOA).	degree
T	Maximum thickness	m
C	Chord length	m
AR	Aspect Ratio	Dimensionless